Applied Catalysis B: Environmental 296 (2021) 120349

Contents lists available at ScienceDirect

Applied Catalysis B: Environmental

journal homepage: www.elsevier.com/locate/apcatb

In situ cofactor regeneration enables selective CO_2 reduction in a stable and efficient enzymatic photoelectrochemical cell

Kaiqi Xu [a], Athanasios Chatzitakis [a,*], Paul Hoff Backe [b,c], Qiushi Ruan [d], Junwang Tang [d,*], Frode Rise [e], Magnar Bjørås [b,f], Truls Norby [a,*]

[a] Centre for Materials Science and Nanotechnology, Department of Chemistry, University of Oslo, FERMiO, Gaustadalléen 21, NO-0349 Oslo, Norway
[b] Department of Microbiology, Oslo University Hospital HF, NO-0372 Oslo, Norway
[c] Department of Medical Biochemistry, Institute for Clinical Medicine, University of Oslo, NO-0372 Oslo, Norway
[d] Department of Chemical Engineering, University College London, Torrington Place, London WC1E 7JE, UK
[e] Department of Chemistry, University of Oslo, NO-0315 Oslo, Norway
[f] Department of Clinical and Molecular Medicine, Faculty of Medicine and Health Sciences, Norwegian University of Science and Technology (NTNU), NO-7491 Trondheim, Norway

ARTICLE INFO

Keywords:
Tantalum nitride
Artificial photosynthesis
Graphitic carbon nitride
NADH regeneration
Formate dehydrogenase

ABSTRACT

Mimicking natural photosynthesis by direct photoelectrochemical (PEC) reduction of CO_2 to chemicals and fuels requires complex cell assemblies with limitations in selectivity, efficiency, cost, and stability. Here, we present a breakthrough cathode utilizing an oxygen tolerant formate dehydrogenase enzyme derived from *clostridium carboxidivorans* and coupled to a novel and efficient *in situ* nicotinamide adenine dinucleotide (NAD^+/NADH) regeneration mechanism through interfacial electrochemistry on g-C_3N_4 films. We demonstrate stable (20 h) aerobic PEC CO_2-to-formate reduction at close to 100 % faradaic efficiency and unit selectivity in a bio-hybrid PEC cell of minimal engineering with optimized Ta_3N_5 nanotube photoanode powered by simulated sunlight with a solar to fuel efficiency of 0.063 %, approaching that of natural photosynthesis.

1. Introduction

Electroreduction of CO_2 to chemicals and liquid fuels not only serves to store excess renewable electricity in chemical bonds but also contributes to CO_2 reduction in the atmosphere [1]. Ideally, the electrical energy can be provided directly by sunlight, mimicking natural photosynthesis. Such photoelectrosynthesis may be of particular importance for dealing with the intermittent nature of sunlight and help mitigate climate change by CO_2 recycling. It faces however challenges related to energy and conversion rate efficiency, product selectivity, cost, and stability of the catalysts.

Many (photo)electrocatalysts have been reported for the production of compounds ranging from two-electron transfer products, CO and HCOOH, to multi-electron transfer ones such as CO, HCOOH, C_2H_4, and alcohols [2–6]. Cu appears to be an important element for the latter class of catalysts [7,8], while electroreductive synthesis of formic acid, HCOOH – an important chemical reagent and insecticide – requires noble-metal or toxic electrocatalysts (Pd, Pt, Au, Pb) [2,3,9,10]. An alternative would be to integrate in the cathode formate dehydrogenase (FDH) enzymes, which selectively catalyze the reduction of CO_2 into formate (HCOOH or $HCOO^-$) [11].

Some FDHs contain W or Mo in their active sites (metal-dependent FDHs) [12] and some of these, such as the ones from *Syntrophobacter fumaroxidans* [13] and *Desulfovibrio vulgaris* [14,15], exhibit fast electron transfer directly from a cathode in electrolytic [13,16] or photoelectrochemical (PEC) cells [15,17]. Direct wiring of electrons across the electrode-protein interface tends to result in high turnover numbers (TONs) [12,18], i.e., fast CO_2 conversion kinetics, but requires that the active sites of the enzymes are exposed or shallow, or connected to the electrode surface by a train of redox cofactors [18], such as FeS clusters. Strictly anaerobic environments are necessary when reducing CO_2, since O_2 easily deactivates those active sites [19]. Despite the high TONs, the stability of directly wired enzymes has not been satisfactory; degradation usually starts immediately following the electron transfer [13,15]. In fact, most enzymes used in industry, including FDHs, cannot be directly wired to electrodes [20], as their functionality relies on the addition of cofactors, such as the nicotinamide adenine dinucleotide (NADH), which is required for most metal-independent FDHs [21,22].

* Corresponding authors.
E-mail addresses: a.e.chatzitakis@smn.uio.no (A. Chatzitakis), junwang.tang@ucl.ac.uk (J. Tang), truls.norby@kjemi.uio.no (T. Norby).

https://doi.org/10.1016/j.apcatb.2021.120349
Received 5 March 2021; Received in revised form 6 May 2021; Accepted 10 May 2021
Available online 13 May 2021

Hence, the coupling of an NADH-dependent oxygen tolerant FDH with an efficient NADH regeneration mechanism will have wide prospects of applications. This is also of great importance to many chemical and pharmaceutical industries, where most of the enzymes involved are dependent on NADH, or its phosphorylated form, NADPH [23]. Therefore, it has been imperative to find an efficient, selective and enzyme-compatible electrode material for NAD(P)H regeneration [20]. Although the addition of a mediator such as the Cp[Rh(5,5′-methyl-2, 2′-bipyridine)] [24] can significantly increase the selectivity by indirect regeneration (introduction of a second redox system), it is burdened by the costs of Rh or other noble metals and the complexity of separation and purification. Moreover, the addition of mediators can cause denaturation of enzymes, leading to diminished activities [25]. Recently, graphitic carbon nitride, g-C_3N_4, studied for its role in solar fuel production [26,27], has shown promising ability to photocatalytically regenerate NADH, both in the presence and absence of mediators [28, 29]. It is believed that the π-π stacking of g-C_3N_4 can interact with the adenine subunit of NAD^+, leading to strong affinity and ability for direct electron transfer and protonation processes between these two substances [28]. This leads to the possibility to directly utilize the g-C_3N_4 as a single electrode, which can be readily used in an electrochemical or PEC cell, eliminating the need of hole scavengers such as triethanolamine (TEOA) and significantly simplifying the separation and purification processes.

Herein and for the first time, a film of g-C_3N_4 on an F-doped SnO_2 (FTO) coated glass was used as an electrode for the direct electrocatalytic NADH regeneration. At the same time, we developed a highly active photoelectrode based on Ta_3N_5 nanotubes, optimized through a simple surface modification procedure. The optimized photoelectrode approaches the theoretical photocurrent density of Ta_3N_5 of approximately 13 mA/cm^2 under solar simulated light and at low overpotential. We have modified the inherently instable Ta_3N_5 [30] to suppress photocorrosion under relatively high photocurrent densities. The two electrodes have then been employed in a bio-hybrid PEC cell, for selective conversion of CO_2 gas to formate with the formate dehydrogenase (FDH) derived from *clostridium carboxidivorans* (*c.c.*) as the biocatalyst. We chose this particular *c.c.* FDH due to its excellent oxygen tolerance, but this comes with the cost that this protein is NADH dependent and has a low turn-over frequency (TOF) [12]. We present however an efficient, selective and facile cofactor regeneration mechanism on this novel cathode, and when powered by the optimized Ta_3N_5 nanotubes, a close to 100 % faradaic efficiency and unity selectivity to formate by CO_2 electroreduction was obtained. We demonstrate a photo-assisted bio--hybrid PEC cell towards artificial photosynthesis, with minimal engineering, under ambient conditions and with an overall efficiency and stability beyond the current state-of-the-art.

2. Experimental section

2.1. Ta_3N_5 NTs photoanode

The growth of Ta_3N_5 NTs is based on our previous works [31,32]. A piece of Ta foil with an area of 0.25 cm^2 was sonicated in a sequence of acetone, isopropanol and DI water for 30 min each, then dried under N_2 stream. The first Ta_2O_5 nanotubes layer was grown under 60 V for 5 min, then rinsed with DI water and removed by an intense airflow from an air compressor. The new Ta_2O_5 nanotubes layer grown under 60 V for 30 min was then stabilized in ethanol for 5 min, before being transferred to a ProboStat™ for nitridation. The conversion of Ta_2O_5 nanotubes to Ta_3N_5 nanotubes was performed by annealing the oxide in a flow of NH_3 (15 sccm) at 950 °C for 2 h, then cooled down under the same NH_3 stream with a rate of 5 °C/min.

2.2. Co-based cocatalysts loading on Ta_3N_5 NTs

The $Co(OH)_x$ cocatalyst was firstly electrodeposited under fixed low current, rather than a fixed potential in order to control a low deposition rate. The deposition was carried out in a 3-electrode electrochemical cell with Ta_3N_5 NTs, standard calomel electrode (SCE) and Pt foil as the working, reference and counter electrodes, respectively. The electrodes were first immersed in a solution containing 0.05 M $Co(NO_3)_2$, of which the pH was carefully adjusted to 11 ± 0.5 by slowly adding 1 M NaOH solution and was constantly monitored by a pH meter (HORIBA D-71 G, Japan). Afterwards, a fixed current of −10 μA/cm^2 was applied on the working electrode for 100 s. The electrodes were then rinsed thoroughly with DI water, before being transferred to another plating solution containing 0.05 mM $Co(NO_3)_2$ in 0.1 M potassium phosphate buffer (pH 7). A potential of 0.85 V vs. SCE was applied on the $Co(OH)_x$ loaded working electrode for 60 s, so that Co-Pi was also loaded.

2.3. g-C_3N_4 porous thin film cathode

g-C_3N_4 thin film (mole ratio of HCl to dicyandiamide = 1) was coated on FTO glass substrate using a thermal evaporation method. For instance, 50 mg dicyandiamide and 0.6 mmol hydrochloride were dissolved with 2 ml DI water. After a thorough stirring, the solution was spread on a 4*4 cm^2 FTO glass substrate and dried in a drying oven at 70 °C for 1 h. The dried precursor (dicyandiamide with hydrochloride) was adhered to the surface of the FTO glass substrate. The substrate was then placed onto a 35 mm diameter petri dish with the precursor side facing downwards. The sample was calcined in a 550 °C preheated muffle furnace (Carbolite, CWF 1300) for 20 min and quenched to room temperature in air. Before tests, the electrodes were masked by Epoxy with an area of 2*2 cm^2 exposed to the electrolytes.

2.4. Enzyme expression and purification

The detailed expression and purification of the *c.c.* FDH is described in the supporting information (SI).

2.5. Electrochemical NADH regeneration and enzymatic CO_2 reduction

Cyclic voltammetry (CV) and chronoamperometry measurements were performed in a 3-electrode configuration under standard atmospheric conditions with or without N_2 bubbling. g-C_3N_4, Pt foil and SCE were used as the working (cathode), counter (anode) and reference electrode, respectively. A Nafion membrane made by soaking 600 u L of 5% Nafion perfluorinated resin solution on a 25 mm diameter cyclopore track etched membrane was set in the middle to separate the anode and cathode chambers. The pores of the cyclopore track etched membrane were fully covered by Nafion as observed by scanning electron microscopy (SEM). As varying buffered solution were used, details can be found in the main document and SI. The reported potentials here were not converted against the reversible hydrogen electrode (RHE) in order to follow the tradition in the literature [20]. The absorption spectrum of 1,4-NADH was monitored with a UV–vis spectrophotometer (SPECORD® 200 PLUS). Data analysis was carried out using the spectroanalytical software WinASPECT PLUS. $^{13}CO_2$ gas was purchased from Merck (99.0 atomic %, 10 L) and was used in the PEC experiments as well. The EnzyChrom™ NAD^+/NADH assay kit (E2ND-100) for the selective detection of 1,4-NADH was purchased from Nordic Diagnostica Service AB, Sweden.

2.6. PEC measurements

PEC water splitting experiments with Ta_3N_5 NTs were performed under standard atmospheric conditions in a 3-electrode configuration with Ta_3N_5 NTs, Pt foil and saturated calomel electrode (SCE) as the photoanode, cathode and reference electrode, respectively, in 1 M NaOH. The AM1.5 G simulated solar light illuminated the 0.25 cm^2 Ta_3N_5 NTs photoanode through a quartz window, and an electronically controlled shutter together with a digital timer was used to generate

intermittent light conditions. The potentials are reported versus RHE using the conversion $E_{RHE} = E_{SCE} + 0.059*pH + 0.244$ V.

PEC CO_2 reduction was performed under a 2-electrode configuration, with Ta_3N_5 NTs as the photoanode and g-C_3N_4/FTO porous thin film as the cathode, under standard atmospheric conditions. The anode and cathode chambers were separated by a Nafion membrane as in the NADH regeneration cell. The photoanode was immersed in PBS solution containing 0.1 M $NaHCO_3$, while the cathode was immersed in PBS solution containing 0.1 M $NaHCO_3$, 2.5 mM NAD^+, ca. 2 mg *c.c.* FDH and purged with CO_2 (0.63 sccm). During the $^{13}CO_2$ labelled experiments, the same solution but without the addition of $NaHCO_3$ was used. The same light source as for the PEC water splitting was used. Further details of instrumentation and product analysis and quantification are provided in SI.

3. Results and discussion

3.1. Ta_3N_5 nanotubes photoanode

The Ta_3N_5 nanotubes (NTs) were synthesized based on our previous method [31], but with removal of the porous non-oriented top layer, see Fig. 1a before and after. This eliminates charge transfer trapping states at the interface between the two layers and increases the surface coverage of the cocatalyst. In our earlier work [32], the optimized cocatalyst was deposited not as a continuous film but rather as randomly dispersed particle islands on the walls of the nanotubes. In this study the electrodeposition of $Co(OH)_x$/Co-Pi with optimized parameters was applied with the first $Co(OH)_x$ layer deposited at fixed low current density (-10 μA/cm^2), resulting in a homogeneous cocatalyst layer covering the entire nanotubes, see Fig. 1b before and after. The bare NTs of smooth surface are known for their photocorrosion during PEC water splitting [30]. Through the modifications, we aimed for enhanced charge transfer kinetics from the surface of the material to the electrolyte while the improved cocatalyst coating can suppress the photocorrosion even under high photocurrent densities.

The current-potential (*j-E*) curves in Fig. 1c show that with the optimized electrodeposition parameters, Ta_3N_5 NTs with Co-based cocatalysts reach 9.4 mA/cm^2 @ 1.23 V vs. RHE under AM1.5 G simulated solar light, the highest reported for Ta_3N_5 NTs, except planar Ta_3N_5 films [33] using rare elements and multiple complicated synthesis steps for a multilayer protection mechanism. At an overpotential of only 100 mV (i.e., 1.33 V vs. RHE) our photocurrent density exceeded 12 mA/cm^2, approaching the theoretical value of 12.9 mA/cm^2. Fig. 1c highlights the material development from the optimization of the electrodeposition parameters of $Co(OH)_x$ and $Co(OH)_x$/Co-Pi dual cocatalyst. Overall, a 50 % increase in the performance of the photoanode was

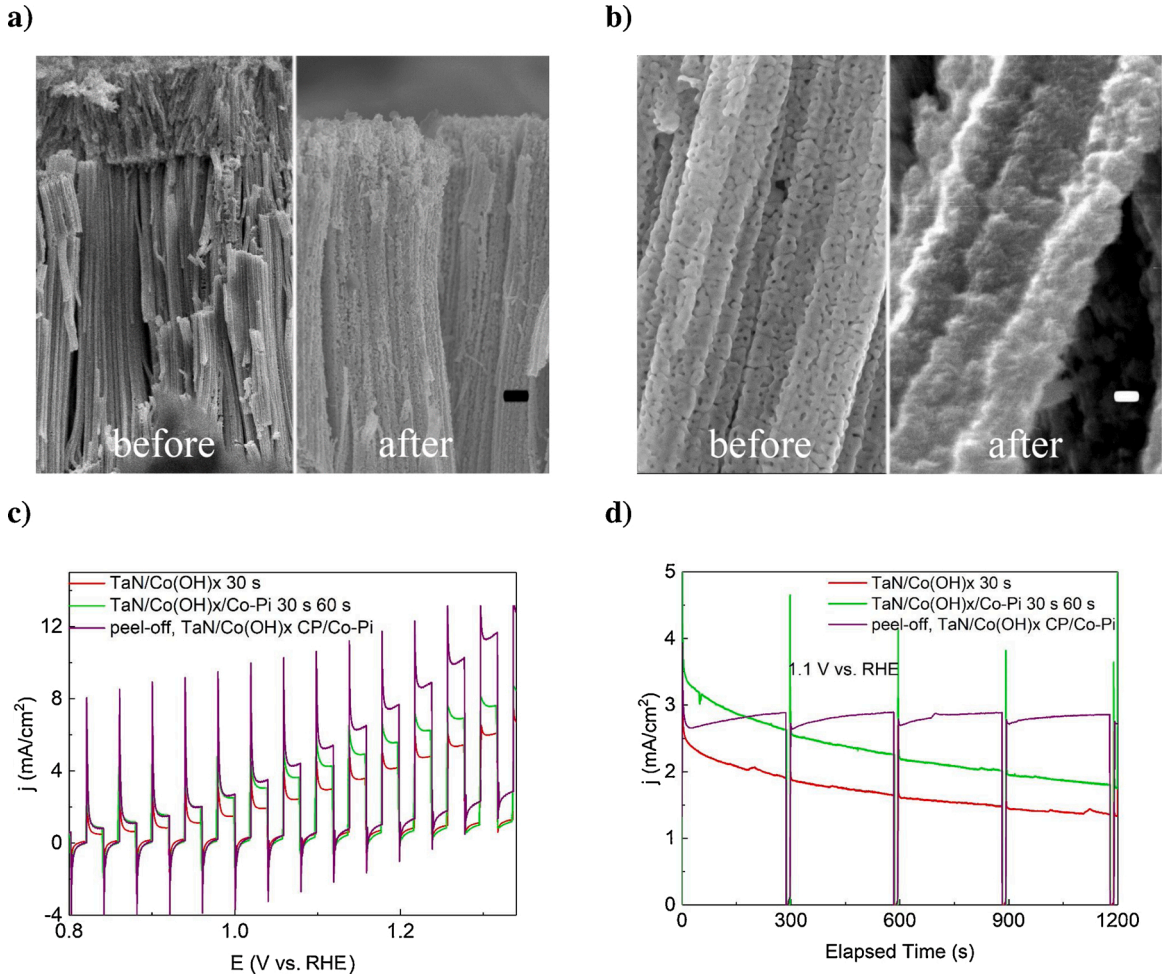

Fig. 1. SEM images of a) Ta_3N_5 NTs array after anodization and ammonolysis, before and after the removal of the top-layer, scale bar 1 μm. b) Before electrodeposition and the smooth surface of NTs. After electrodeposition a homogenous yet rough cocatalyst layer is present fully covering the NTs, scale bar 100 nm. c) *j-E* curve of Ta_3N_5 NTs with electrodeposited $Co(OH)_x$/Co-Pi cocatalysts reaching 9.4 mA/cm^2 @ 1.23 V vs. RHE under AM1.5G simulated solar light (purple curves). The red and green curves are parts of the history of the development of the material as previously published [31,32]. d) Optimized Ta_3N_5 NTs (purple curve) stabilized at 3 mA/cm^2 under 1.1 V vs. RHE for at least 20 min. Again, the red and green curves highlight the comparative degradation of the material without surface optimization of the underlying nitride. (For interpretation of the references to colour in this figure legend, the reader is referred to the web version of this article).

achieved by these simple and robust modifications. A long-term PEC water splitting experiment was undertaken and an overall faradaic efficiency of measured oxygen evolution as high as 90 % was reached over 3 h, indicating a dramatically reduced photocorrosion (Fig. S2a). A supplementary video is also given in the SI, where the O_2 gas release from the surface modified Ta_3N_5 NTs photoanode is highlighted.

As expected, the improved cocatalyst coverage of the underlying nitride surface resulted in a significantly improved stability at relatively lower photocurrent densities. The purple curve in Fig. 1d shows that at 3 mA/cm^2 (@ 1.1 V vs. RHE) the performance has been maintained for 20 min without any noticeable decay. A direct rerun of the stability test shows that this performance was maintained at least for another 20 min, and decreased to 52 % of its initial performance after more than 3 h total test period (Fig. S3). At this point, post-operation SEM shows a significant deformation of the Ta_3N_5 NTs and loss of the continuous and homogeneous cocatalyst layer, as seen in Fig. S4. Additionally, the XRD pattern of the degraded sample (Fig. S5 blue curve) shows the evolution of several new diffraction peaks, implying the formation of secondary phases most likely related to the formation of TaO_x [34]. On the other hand, this is the longest stable performance achieved for nanotubular structured Ta_3N_5-based photoelectrodes, in stark contrast to the non-optimized samples, where around 50 % loss in the stability was observed after only 20 min of operation. Nevertheless, it could be that electrodeposition of the cocatalyst on such high aspect ratio nanostructures may not be the most appropriate method, as any uncoated surface can serve as a corrosion point. Other techniques, such as atomic layer deposition (ALD) or further development of the facile electrodeposition method should be pursued.

While our optimized Ta_3N_5 NTs decorated with Co-based dual cocatalyst can yield high photocurrent densities, a better stability is achieved at moderate current densities, e.g., 1 mA/cm^2 (Fig. S2b). A PEC with a biocatalyst (enzyme) replacing noble metals will operate at and tolerate only lower current densities although they can show relatively high turnover numbers (TONs) [35,36]. For these reasons we developed a novel bio-hybrid cathode for enzymatic selective reduction of CO_2 to formate and show subsequently how we drive it with our optimized Ta_3N_5 NTs photoelectrode.

3.2. Bio-hybrid cathode based on g-C_3N_4 and FDH enzyme

The cofactor (NADH) dependent *c.c.* FDH enzyme that we have chosen here, has shown good activity in ambient environments with presence of oxygen [37] as confirmed also in our lab (Fig. S6). Additional information regarding the enzyme structure, stability, and activity, together with a short description regarding the possible CO_2 reduction mechanism by metal-dependent and –independent FDH enzymes, can be found in SI in Figs. S7 and S8 and corresponding analysis. Although the *c.c.* FDH enzyme is oxygen tolerant, its utilization has been little reported, and we have only found one work integrating the *c.c.* FDH as the first step in a cascade enzymatic system [38]. The main reason may be the low TOF for this enzyme in CO_2 reduction [12]. However, its long lifetime [37] and modest requirements during operation make this enzyme suitable for up-scaling.

Preliminary synthesis in our laboratories have shown that the ratio between HCl and dicyandiamide (DCDA) has an impact on the morphology of the g-C_3N_4 film (Fig. S9 and corresponding analysis). Herein, the 1:1 ratio of HCl and DCDA was used in order to produce a porous g-C_3N_4 film electrode, as described in the experimental section [27]. The cross sectional SEM images (Figs. S9 and S10a) show a 5 μm thick, porous g-C_3N_4 film directly coated on the FTO substrate (g-C_3N_4/FTO). Such a g-C_3N_4/FTO electrode shows a typical *j-E* curve of an n-type semiconductor under light on-off cycles when the potential is relatively positive (-0.2∼-0.3 V vs. RHE), while no obvious p-type semiconductor properties are evident at more negative potentials (Fig. S10b). This indicates that the direct utilization of such an electrode as a photocathode is not applicable, hence we used the g-C_3N_4/FTO as a regular cathode and substrate for the NADH mediated electron transfer to FDH.

The electrocatalytic activity of the g-C_3N_4/FTO electrode towards the selective NADH regeneration to the enzymatically active form of 1,4-NADH is studied by CV, UV–vis spectroscopy and enzymatic detection methods. The study was conducted in a two-compartment electrolytic cell in which the cathode side contained 2.5 mM NAD^+ under continuous supply of N_2 gas. Fig. 2a shows distinct differences in the voltammetric behavior of the porous g-C_3N_4 in the absence and presence of NAD^+. A clear reduction peak at -1.16 V vs. SCE (pH 8.5) under a scanning rate of 100 mV/s is assigned to the NAD^+/NADH redox couple, which is not present when there is no NAD^+ in the electrolytic buffer solution (green dashed line). The formal potential for the NAD^+/NADH redox couple is at −0.56 V vs. SCE, so an overpotential of approx. 0.6 V is required that is amongst the lowest reported for similar systems of direct electron transfer [20,39]. At more negative potentials electrocatalytic hydrogen evolution occurs. Reversing the potential scan direction an oxidation peak is observed at -0.80 V vs. SCE that is assigned to hydrogen desorption, which is rather important, as it suggests that protons are present in the reaction sites for the hydrogenation of NAD^+. Such a CV profile has been seen in other systems for example in Ru nanoparticles on glassy carbon [40].

A very different behavior is seen for the FTO substrate as revealed by Fig. S11a, where the reduction peak of NAD^+ is moved to −1.39 V vs. SCE at 100 mV/s. Moreover, there is no clear hydrogen desorption peak during the reverse scan towards less reducing potentials. This behavior fits with a previous report on the influence of FTO coated glass for the NADH regeneration reaction [41]. It should be noted that the authors did not provide any evidence for the selective reduction of NAD^+ to 1, 4-NADH. Therefore, FTO can irreversible reduce NAD^+ and this is evident from the linear dependence of the peak potential (E_p) and the changing shape of the voltammetric profile from the scan rate, as given in Fig. S12a. A similar linear dependence is also observed for the peak current density (j_p) from the scan rate (Fig. S12b), suggesting a diffusion controlled reduction reaction on the surface of the electrode. The same trend follows also the dependence of the peak potential and peak current density on the scan rate for the hydrogen desorption peak as seen in Fig. S12c and d.

In order to investigate the formation of the enzymatically active 1,4-NADH for both the g-C_3N_4/FTO and bare FTO electrodes, we conducted chronoamperometric experiments at potentials close to the respective peak potential as given in Fig. 2b and Fig. S11b. The steady state current densities fit well with the expected ones from the CV profiles for both electrodes. The absorption spectra of the cathode compartment electrolytic solution was then monitored and the evolution of the characteristic peak at 340 nm for the 1,4-NADH is clearly seen for both electrodes (Figs. 2c and S11c). The reference absorption spectra of commercially available 1,4-NADH and the respective reference peak are given in Fig. S13a and b. We further confirmed the selective formation of 1,4-NADH (Fig. S13c and d) with the use of the commercially available test kit EnzyChrom™, according to the procedure described by Saba et al. [42] The yields regarding the selective formation of 1,4-NADH are presented in Table S1 and a linear increase of its concentration is observed for both electrodes in good accordance with their steady state current densities of Figs. 2b and S11b. On the other hand, g-C_3N_4 has a 2–3 times better faradaic efficiency (FE) compared to the bare FTO, as found after integration of the chronoamperometric curves at each time interval.

We investigated the effect of the pH and the absence of bicarbonates in the electrolytic solution on the CV behavior of g-C_3N_4/FTO in electrolyte containing dissolved oxygen but also in electrolyte flushed with N_2. As seen from Figs. 2d and S14a, the CV profile is slightly altered with the NAD^+ reduction peak moving to −1.01 V vs. SCE (0.150 V more positively instead of 0.084 V as expected for a pH difference of 1.4) and the hydrogen desorption peak to −0.66 V vs. SCE (0.014 V instead of 0.084). Thus, we observe a non-Nernstian behavior, which can be found

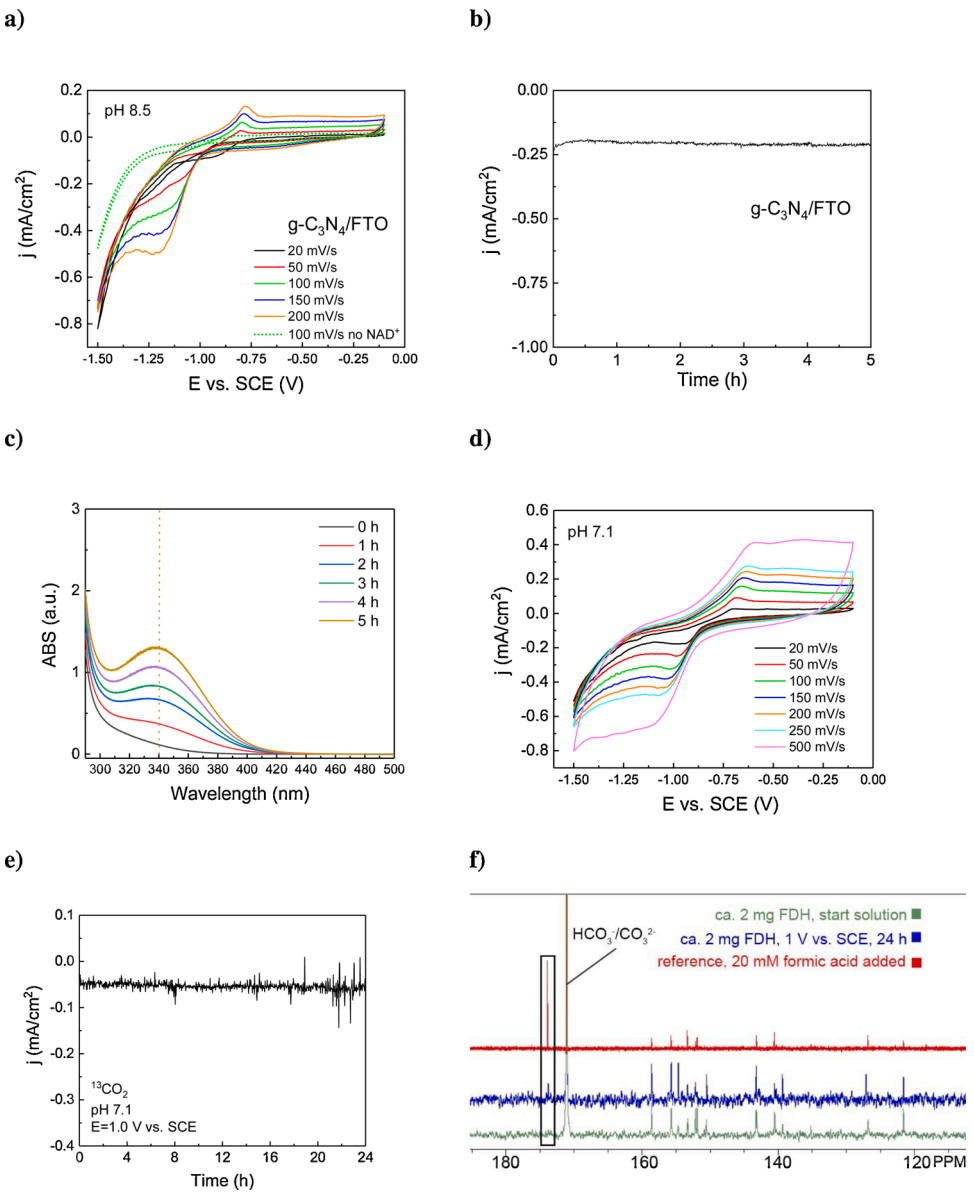

Fig. 2. a) CV of g-C_3N_4/FTO as working electrode (cathode) in a dual compartment electrochemical cell, which the cathode compartment was bubbled with N_2 gas. The reference electrode in the cathode compartment was SCE, while anode was a Pt mesh. A Nafion membrane was used to separate the two compartments. The cathode side contained 2.5 mM NAD^+, 0.1 M $NaHCO_3$ in PBS (pH 8.5). The Pt anode solution contained 0.1 M $NaHCO_3$ in PBS. The stabilized cycles are only shown that were obtained after at least 5 cycles. b) NAD^+ electroreduction at the peak potential (E_p=1.20 V vs. SCE) with g-C_3N_4/FTO as working electrode. c) Absorption spectra of the cathode solution from the electroreductive experiment of b). d) CV profiles of g-C_3N_4/FTO as working electrode (cathode) in a dual compartment electrochemical cell with as prepared PBS (pH 7.1). In this case no bicarbonates were used in both anode and cathode buffer solutions. Cathode contained 2.5 mM NAD^+. e) Electroreduction of $^{13}CO_2$ at the NAD^+/NADH peak potential (E_p=1.0 V vs. SCE) with g-C_3N_4/FTO as working electrode. The cathode solution contained ca. 2 mg FDH enzyme, 2.5 mM NAD^+, in PBS (pH 7.1) and bubbled with $^{13}CO_2$ with a flow of 1.8 mL/min. f) ^{13}C NMR spectra of the solution after 0 h and 24 h labelled experiment of e), 20 mM formic acid were added as the reference ^{13}C spectrum. The highlighted peak at 173.84 ppm after 24 h labelled experiment, is assigned to the formate production by $^{13}CO_2$ reduction (blue), as correlated by addition of the internal standard (red). (For interpretation of the references to colour in this figure legend, the reader is referred to the web version of this article).

in irreversible processes that thermodynamic equilibrium cannot be reached [43]. This result agrees well with the fact that the E_p for both processes moves negatively with increasing scan rate as seen in Fig. S14b. In agreement with the CV measurements at pH 8.5 a linear dependence of the peak current density with the scan rate is observed (Fig. S14c), denoting diffusion control reactions. Similar linear dependence of the E_p and j_p for the hydrogen desorption process with the scan rate was also found (see Fig. S14d and e). The results as calculated by Eq. 2 and 3 in the SI are given in Table S2 revealing a lower diffusion coefficient for the g-C_3N_4 electrode that is assigned to its porosity compared to the relatively flat FTO surface. Moreover, the D_o values in the range of 10^{-6} cm^2/s are in perfect agreement with the expected values presented in the literature [44–46].

Finally, we performed a 24 h long experiment in the NADH regeneration two-compartment cell in the presence of the FDH enzyme under a low flow of labelled $^{13}CO_2$ gas. We highlight the absence of bicarbonates, therefore the only carbon source was the labelled CO_2 gas stream. The chronoamperometric curve of Fig. 2e suggests a stable operation of the NADH regeneration cell, which in the presence of FDH the characteristic absorption peak of 1,4-NADH at 340 nm was not observed (Fig. S14f). Importantly, ^{13}C NMR measurements clearly show the evolution of a ^{13}C peak related to the formation of $H^{13}COO^-$ (Fig. 2f). This experiment not only provides additional evidence for the successful formation of enzymatically active 1,4-NADH, but it also highlights the synthesis of formate directly from CO_2 gas.

3.3. Hybrid PEC cell assembly and CO_2 reduction

A PEC cell with the optimized Ta_3N_5 NTs modified with Co species as cocatalyst and the g-C_3N_4/FTO cathode was assembled according to the schematic depicted in Fig. 3a. A total amount of 2 mg *c.c.* FDH enzyme was distributed in the cathode PBS solution containing 0.1 M $NaHCO_3$ and 2.5 mM NAD^+, while CO_2 was continuously purged as feedstock. The g-C_3N_4/FTO cathode with an exposed area of 4 cm^2 was immersed and the assembly was left under ambient conditions. A proton conducting Nafion membrane is set in the middle to separate the two chambers. The optimized Ta_3N_5 NTs photoanode was immersed in the anode side of the PEC assembly, in the same PBS solution without NAD^+ or the enzyme. During the PEC operation for CO_2 reduction, only the photoanode received the AM1.5 G simulated solar light through a quartz window. The conduction band (CB) of g-C_3N_4 is 0.3 eV more negative than that of Ta_3N_5, and a bias, V_{app} was hence needed and applied in

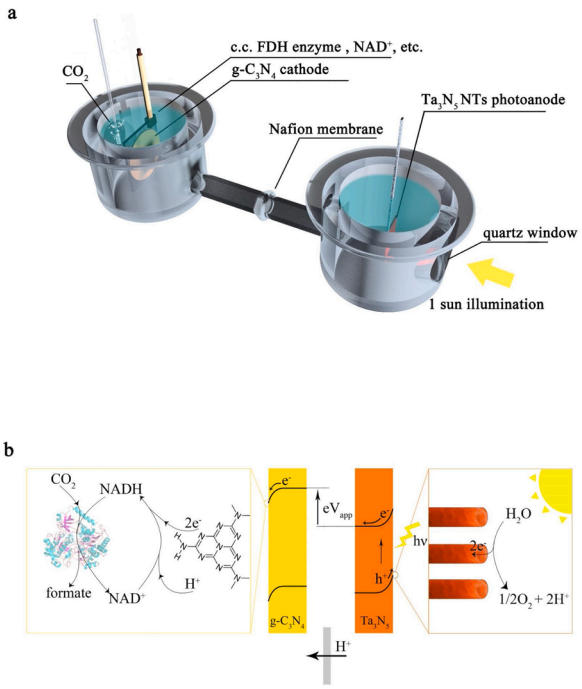

Fig. 3. a) Schematic of the *c.c.* FDH integrated bio-hybrid PEC cell. Cathode: g-C_3N_4/FTO immersed in a 60 mL solution containing ca. 2 mg *c.c.* FDH, 2.5 mM NAD^+, 0.1 mM $NaHCO_3$, in PBS solution and purged with CO_2. Photoanode: Ta_3N_5 NTs with top layer removed, $Co(OH)_x$ deposited at -10 μA/cm^2 for 100 s, and Co-Pi under 0.85 V vs. SCE for 60 s, immersed in 60 mL PBS solution containing 0.1 mM $NaHCO_3$. Top fittings for both compartments were used but not depicted for simplicity. b) charge transfer pathways for the whole PEC cell.

order to successfully inject the photo-generated electrons from the CB of Ta_3N_5 to that of g-C_3N_4.

Fig. 3b shows the charge transfer pathways of the whole PEC system. Electron-hole pairs are generated close to the surface of the Ta_3N_5 NTs and get separated at the space charge region (SCR), where after electrons move to the bulk and holes to the surface. The 1D nature of nanotubes may not only increase the surface area, but also improve the charge separation efficiency by allowing electrons and holes to move in opposite directions [47]. Water molecules will be oxidized by the photo-generated holes at the surface of the photoanode, evolving oxygen gas and protons diffusing through the electrolyte towards the cathode. The photo-generated electrons gain an energy of eV_{app} by assistance of external bias and are injected to the CB of the g-C_3N_4, where they are transferred to NAD^+ most probably through the interaction between the π-π stacking of g-C_3N_4 and the adenine subunit of NAD^+ [28]. At the same time, NAD^+ is protonated, leading to the regeneration of NADH. With *c.c.* FDH enzyme and dissolved CO_2 readily available, direct CO_2 reduction to formate takes place.

The transient photocurrent density curve of the 2-electrode hybrid PEC cell in Fig. 4a shows a photocurrent onset of ca. 0.2 V in good agreement with the CB difference. However, the photocurrent is low when compared to the high performance of several mA/cm^2 obtained earlier in PEC water splitting, where only inorganic catalysts were evolved. This is due to the mismatch of the CBs of Ta_3N_5 and g-C_3N_4, therefore extra bias is required to pump the electrons coming from the photoanode to the cathode. In addition, g-C_3N_4 is a poor conductor [48] imposing considerable ohmic overpotential losses. Moreover, there are overpotentials from the finite kinetics of NADH regeneration and CO_2 reduction via the FDH enzyme [20]. Thus, it is reasonable to assume that electrons are suffering from poor mobility and low charge transfer kinetics at the cathode, therefore, most of the photo-generated electron--hole pairs in Ta_3N_5 are recombined, leading to a significant photocurrent decrease. This behavior correlates well with the more intense anodic photocurrent transients, which are significant even at 1.6 V vs. g-C_3N_4, suggesting that in this system the recombination of charge carriers is mostly due to electron accumulation in the bulk of the Ta_3N_5 NTs photoanode. This is not the case when Pt is used as the cathode electrode (refer to Fig. 1), although a direct comparison is avoided, as the Pt cathode was used in a 3-electrode configuration.

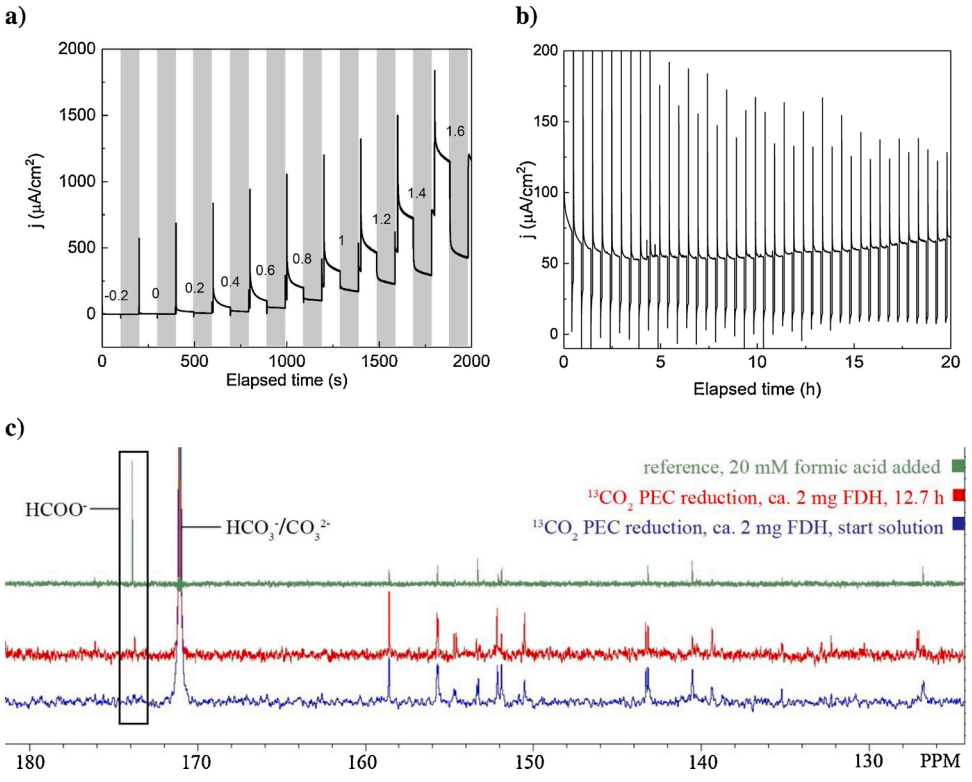

Fig. 4. a) Transient photocurrent density of a hybrid PEC cell assembly with different applied voltage (indicated by the numbers) under 100 s light on (light bar) and off (grey bar) cycles, b) Photocurrent density of CO_2 reduction by the *c.c.* FDH enzyme integrated PEC cell, with 1 V applied bias in a 2-electrode setup for 20 h. c) ^{13}C NMR spectra of the cathode solution in a $^{13}CO_2$ labelled PEC experiment with no addition of $NaHCO_3$. (For interpretation of the references to colour in this figure legend, the reader is referred to the web version of this article).

The photocurrent density shown here is still among the highest reported and with much better stability than hybrid systems reported in the literature, which rarely contain a long-term PEC stability test (Table S3) [15,17]. In order to test the stability and the production of formate in our system, a 20 h PEC CO_2 reduction was performed under 1 V applied bias under ambient (aerobic) conditions, with 5 min light off and 25 min light on cycles, as shown in Fig. 4b. Overall, the photocurrent shows a good stability and after an initial decrease stays constant until an increasing trend starts after some 10 h. XRD of the post operation photoanode (Fig. S5 red curve) further confirms the retention of the crystal structure and that no secondary phases appeared, as opposed to the photoanode operated at high current densities (Fig. S5 blue curve). One possible reason for the initial photocurrent decrease is the Co leaching from the $Co(OH)_x$/Co-Pi cocatalyst. This correlates well with the relatively larger cathodic photocurrent transients, as shown in Fig. S15a, suggesting hole accumulation due to Co leaching. Then a redeposition of Co can take place in the phosphate buffer during the following hours [49], so that hole transfer is improved again and an increase in the photocurrent is witnessed. This is in agreement with the observation that cathodic photocurrent transients diminish after the 10 h, see Fig. S15b. Moreover, SEM of the nanotube electrode operating at low current densities during the bio-hybrid PEC testing (Fig. S15c) shows a retention of the initial morphology, in stark contrast to the deformed nanotubes operating at high current densities (Fig. S4b).

The solution at the cathode was collected at specific intervals and analyzed with NMR. The ^{1}H NMR spectra (Fig. S16) clearly shows production of formate. The emerging peak at chemical shift 8.44 ppm is assigned to the presence of formate according to the internal reference spectrum, in good agreement with all the previous ^{1}H NMR spectra containing formate. A control test operated under the same conditions but without the addition of *c.c.* FDH was also carried out, and the corresponding ^{1}H NMR spectrum (Fig. S16) shows no peak for formate, in evidence that the enzyme is necessary in the cathode for CO_2 electroreduction.

The theoretical faradaic formate production was calculated by integrating the photocurrent density in Fig. 4b, yielding an expected 5 μmol of formate. From the NMR spectra, an amount of 4.9 μmol of formate was found according to the standard curve (Fig. S17), i.e. at 100 % FE within the applicable uncertainty. This means that both the enzymatic CO_2 reduction and NADH regeneration steps are highly selective. The calculated solar-to-fuel (STF) efficiency (refer to SI for the calculations) in which the applied bias is extracted and the photons from the whole solar simulated spectra are considered, is 0.063 %, as compared with the average efficiency of 0.1 % of natural photosynthesis [50,51]. We performed the experiment in the presence of $^{13}CO_2$ as the sole carbon source in order to prove the direct CO_2 utilization by FDH in our hybrid PEC cell. Due to the long acquisition time for ^{13}C NMR spectra, we added NaOH (0.1 M final concentration) in the measurement sample solution to deactivate the FDH enzyme, while the rest of the conditions were kept the same as for the initial experiment. After 12.7 h PEC $^{13}CO_2$ reduction, a peak emerged at 173.86 ppm. According to the reference spectrum with 20 mM formic acid as the internal reference, we confirmed the direct formate production from $^{13}CO_2$ reduction. The peak at 171.08 ppm next to the formate is related to $H^{13}CO_3^-/^{13}CO_3^{2-}$ [52], resulting from the reaction of dissolved $^{13}CO_2$ with NaOH.

Currently, the most common commercialized method for cofactor regeneration is to use enzymes, such as the glucose dehydrogenases (GDHs) or FDHs [53], to protonate and reduce NAD^+ to 1,4-NADH by oxidizing sacrificial substrates glucose or formic acid [54]. This requires costly downstream separation and purification, and suffers from the instability of most enzymes, resulting in the high prices of NADH and NADPH (10^{5-6} USD/mol) [20]. New paths of cofactor regeneration comprise chemical, catalytic (homogenous and heterogeneous), photocatalytic, and electrochemical methods, but they all suffer from drawbacks including poor selectivity or stability, bio-incompatibility, or separation and purification difficulties [20]. The electrochemical method developed herein based on non-toxic, stable and inexpensive g-C_3N_4 warrants further studies to enhance its electronic conductivity and performance not only in bio-hybrid PEC systems, but also unravel the underlying mechanisms for use in the selective regeneration of the enzymatically active 1,4-NADH. Although we have not currently shown a 100 % FE of the g-C_3N_4/FTO electrode for the selective 1,4-NADH generation but rather around 25–30 %, we note that the FE is strongly dependent on the applied potential, and these two systems are not comparable due to different operating conditions. In the PEC system a 2-electrode configuration was used and the electrons are pumped from the CB of the Ta_3N_5 photoanode. In the electrocatalytic experiment, a 3-electrode configuration was used to study the regeneration mechanism and extract the thermodynamic and kinetic data. Furthermore, the actual applied voltage and current density play an important role in the selectivity and conversion efficiency, parameters that should be further pursued and studied. Among the highest reported direct regenerating cathode electrodes are glassy carbon deposited with Pt or Ni nanoparticles [55]. Under a certain potential range a 100 % yield in 1, 4-NADH have been achieved with such electrodes, but the FE was not reported. From the presented *j-E* curves we have calculated a 26 % FE for the glassy carbon-Pt electrode that reflects the high activity of our g-C_3N_4/FTO electrode.

In order to further interrogate our results, we repeated the hybrid PEC experiment of Fig. 4 at 1.3 V vs. cathode and a linear evolution of the formate concentrations was observed (see Fig. S18). We emphasize the stability of our g-C_3N_5 film electrode, which showed no apparent morphology change (Fig. S19) taken into account that it was used for several and lengthy experiments under the presented electrocatalytic and hybrid PEC conditions. We also emphasize the stability of our *c.c.* FDH enzyme, which maintains 75 % of its activity after standing for 48 h under normal atmospheric conditions (Fig. S7).

4. Conclusions

With our optimized dual Co-based cocatalyst, Ta_3N_5 nanotubes facilely fabricated from earth-abundant elements exhibit a high performance of 9.4 mA/cm^2 @ 1.23 V vs. RHE under 1 sun and improved stability towards photocorrosion. For its integration in bio-hybrid PECs, it is moreover important that the conduction band of Ta_3N_5 is quite negative compared to other photocatalysts like TiO_2, Fe_2O_3 and $BiVO_4$ (Fig. S20), whereby lower overpotentials – here 1 V – are needed in order to electrochemically reduce CO_2 while oxidation of water is still favorable from the band positioning. Ta_3N_5 is in itself prone to photocorrosion at high current densities, but we have demonstrated that fine tuning the electrodeposition parameters of the cocatalyst can improve the surface kinetics and at the same time protect the underlying material by efficiently extracting the photogenerated holes, yielding viable stability under the modest current densities of enzymatic photoelectrosynthesis.

It is not common to see STF efficiencies of reported bio-hybrid photoelectrocatalytic systems [56,57], with the exception of 0.08 ± 0.01 % from Wang et al. [58], 0.042 % from the work of Lee et al. [59] and 0.02 % from Andrei et al., [60] with the latter reporting on syngas formation rather than formate. Therefore, our STF efficiency of 0.063 % is amongst the highest reported so far in a bio-hybrid PEC system of minimal engineering, operated stably (20 h) under the total solar irradiance and normal atmospheric conditions.

Author contributions

K.X. Conceptualization, Methodology, Validation, Investigation, Writing – Original Draft & Editing, Visualization, **A.C.** Conceptualization, Methodology, Validation, Investigation, Writing – Original Draft & Editing, Visualization, Supervision, Project Administration, Funding Acquisition, **P.H.B.** Conceptualization, Methodology, Investigation, Validation, Writing – Original Draft & Editing, Supervision, Funding

Acquisition, **Q.R.** Conceptualization, Methodology, Investigation, **J.T.** Conceptualization, Methodology, Validation, Supervision, **F.R.** Methodology, Supervision, **M.B.** Conceptualization, Methodology, Supervision, Funding Acquisition, **T.N.** Conceptualization, Methodology, Writing – Original Draft, Review & Editing, Supervision, Project Administration, Funding Acquisition.

Declaration of Competing Interest

The authors declare that they have no known competing financial interests or personal relationships that could have appeared to influence the work reported in this paper.

Acknowledgements

This work was supported by the Research Council of Norway (RCN) project "CO2BiOPEC" (250261), the Norwegian NMR Package in 1994, and the Norwegian NMR Platform, NNP (226244/F50). K.X. and A.C. acknowledge support from the European Research Council (ERC) under the European Union's Horizon 2020 research and innovation program (grant agreement No 856446 "CUBE") and RCN project "PH2ON" (288320), respectively, during the finalization process.

Appendix A. Supplementary data

Supplementary material related to this article can be found, in the online version, at doi:https://doi.org/10.1016/j.apcatb.2021.120349.

References

[1] Y.Y. Birdja, E. Pérez-Gallent, M.C. Figueiredo, A.J. Göttle, F. Calle-Vallejo, M.T. M. Koper, Advances and challenges in understanding the electrocatalytic conversion of carbon dioxide to fuels, Nat. Energy 4 (2019) 732–745.
[2] Y. Hori, H. Wakebe, T. Tsukamoto, O. Koga, Electrocatalytic process of CO selectivity in electrochemical reduction of CO_2 at metal electrodes in aqueous media, Electrochim. Acta 39 (1994) 1833–1839.
[3] X. Min, M.W. Kanan, Pd-catalyzed electrohydrogenation of carbon dioxide to formate: high mass activity at low overpotential and identification of the deactivation pathway, J. Am. Chem. Soc. 137 (2015) 4701–4708.
[4] H. Yano, T. Tanaka, M. Nakayama, K. Ogura, Selective electrochemical reduction of CO_2 to ethylene at a three-phase interface on copper(I) halide-confined Cu-mesh electrodes in acidic solutions of potassium halides, J. Electroanal. Chem. 565 (2004) 287–293.
[5] M. Le, M. Ren, Z. Zhang, P.T. Sprunger, R.L. Kurtz, J.C. Flake, Electrochemical reduction of CO_2 to CH_3OH at copper oxide surfaces, J. Electrochem. Soc. 158 (2011) E45–E49.
[6] D. Ren, Y. Deng, A.D. Handoko, C.S. Chen, S. Malkhandi, B.S. Yeo, Selective electrochemical reduction of carbon dioxide to ethylene and ethanol on copper(I) oxide catalysts, ACS Catal. 5 (2015) 2814–2821.
[7] P. Iyengar, J. Huang, G.L. De Gregorio, C. Gadiyar, R. Buonsanti, Size dependent selectivity of Cu nano-octahedra catalysts for the electrochemical reduction of CO_2 to CH_4, Chem. Commun. 55 (2019) 8796–8799.
[8] G. Mangione, J. Huang, R. Buonsanti, C. Corminboeuf, Dual-facet mechanism in copper nanocubes for electrochemical CO_2 reduction into ethylene, J. Phys. Chem. Lett. 10 (2019) 4259–4265.
[9] Y. Tamaki, T. Morimoto, K. Koike, O. Ishitani, Photocatalytic CO2 reduction with high turnover frequency and selectivity of formic acid formation using Ru (II) multinuclear complexes, Proc. Natl. Acad. Sci. 109 (2012) 15673–15678.
[10] R. Kortlever, I. Peters, S. Koper, M.T.M. Koper, Electrochemical CO_2 reduction to formic acid at low overpotential and with high faradaic efficiency on carbon-supported bimetallic Pd–Pt nanoparticles, ACS Catal. 5 (2015) 3916–3923.
[11] T.W. Woolerton, S. Sheard, Y.S. Chaudhary, F.A. Armstrong, Enzymes and bio-inspired electrocatalysts in solar fuel devices, Energy Environ. Sci. 5 (2012) 7470–7490.
[12] L.B. Maia, I. Moura, J.J. Moura, Molybdenum and tungsten-containing formate dehydrogenases: aiming to inspire a catalyst for carbon dioxide utilization, Inorg. Chim. Acta 455 (2017) 350–363.
[13] T. Reda, C.M. Plugge, N.J. Abram, J. Hirst, Reversible interconversion of carbon dioxide and formate by an electroactive enzyme, Proc. Natl. Acad. Sci. 105 (2008) 10654–10658.
[14] S.M. da Silva, J. Voordouw, C. Leitao, M. Martins, G. Voordouw, I.A. Pereira, Function of formate dehydrogenases in Desulfovibrio vulgaris Hildenborough energy metabolism, Microbiology 159 (2013) 1760–1769.
[15] K.P. Sokol, W.E. Robinson, A.R. Oliveira, J. Warnan, M.M. Nowaczyk, A. Ruff, I. A. Pereira, E. Reisner, Photoreduction of CO_2 with a formate dehydrogenase driven by photosystem II using a semi-artificial Z-scheme architecture, J. Am. Chem. Soc. 140 (2018) 16418–16422.
[16] K. Sakai, Y. Kitazumi, O. Shirai, K. Takagi, K. Kano, Direct electron transfer-type four-way bioelectrocatalysis of CO_2/formate and NAD^+/NADH redox couples by tungsten-containing formate dehydrogenase adsorbed on gold nanoparticle-embedded mesoporous carbon electrodes modified with 4-mercaptopyridine, Electrochem. Commun. 84 (2017) 75–79.
[17] K.P. Sokol, W.E. Robinson, J. Warnan, N. Kornienko, M.M. Nowaczyk, A. Ruff, J. Z. Zhang, E. Reisner, Bias-free photoelectrochemical water splitting with photosystem II on a dye-sensitized photoanode wired to hydrogenase, Nat. Energy 3 (2018) 944.
[18] C. Léger, P. Bertrand, Direct electrochemistry of redox enzymes as a tool for mechanistic studies, Chem. Rev. 108 (2008) 2379–2438.
[19] J. Fritsch, P. Scheerer, S. Frielingsdorf, S. Kroschinsky, B. Friedrich, O. Lenz, C. M. Spahn, The crystal structure of an oxygen-tolerant hydrogenase uncovers a novel iron-sulphur centre, Nature 479 (2011) 249.
[20] X. Wang, T. Saba, H.H. Yiu, R.F. Howe, J.A. Anderson, J. Shi, Cofactor NAD (P) H regeneration inspired by heterogeneous pathways, Chem 2 (2017) 621–654.
[21] V.O. Popov, V.S. Lamzin, NAD(+)-dependent formate dehydrogenase, Biochem. J. 301 (Pt 3) (1994) 625–643.
[22] A. Alekseeva, S. Savin, V. Tishkov, NAD^+-dependent formate dehydrogenase from plants, Acta Naturae 3 (2011).
[23] U. Bornscheuer, G. Huisman, R.J. Kazlauskas, S. Lutz, J. Moore, K. Robins, Engineering the third wave of biocatalysis, Nature 485 (2012) 185.
[24] F. Hildebrand, C. Kohlmann, A. Franz, S. Lütz, Synthesis, characterization and application of new rhodium complexes for indirect electrochemical cofactor regeneration, Adv. Synth. Catal. 350 (2008) 909–918.
[25] Y.J. Yoo, Y. Feng, Y.H. Kim, C.F.J. Yagonia, Regeneration of Cofactors, Fundamentals of Enzyme Engineering, Springer, 2017, pp. 49–58.
[26] S. Kumar, S. Karthikeyan, A.F. Lee, g-C_3N_4-based nanomaterials for visible light-driven photocatalysis, Catalysts 8 (2018) 74.
[27] Q. Ruan, W. Luo, J. Xie, Y. Wang, X. Liu, Z. Bai, C.J. Carmalt, J. Tang, A nanojunction polymer photoelectrode for efficient charge transport and separation, Angew. Chemie Int. Ed. 56 (2017) 8221–8225.
[28] J. Liu, M. Antonietti, Bio-inspired NADH regeneration by carbon nitride photocatalysis using diatom templates, Energy Environ. Sci. 6 (2013) 1486–1493.
[29] J. Liu, J. Huang, H. Zhou, M. Antonietti, Uniform graphitic carbon nitride nanorod for efficient photocatalytic hydrogen evolution and sustained photoenzymatic catalysis, ACS Appl. Mater. Interfaces 6 (2014) 8434–8440.
[30] Y. He, J.E. Thorne, C.H. Wu, P. Ma, C. Du, Q. Dong, J. Guo, D. Wang, What limits the performance of Ta_3N_5 for solar water splitting? Chem 1 (2016) 640–655.
[31] K. Xu, A. Chatzitakis, I.J.T. Jensen, M. Grandcolas, T. Norby, $Ta_3N_5/Co(OH)_X$ composites as photocatalysts for photoelectrochemical water splitting, Photochem. Photobiol. Sci. 18 (2019) 837–844.
[32] K. Xu, A. Chatzitakis, S. Risbakk, M. Yang, P.H. Backe, M. Grandcolas, M. Bjørås, T. Norby, High performance and toxicity assessment of Ta3N5 nanotubes for photoelectrochemical water splitting, Catal. Today 361 (2021) 57–62.
[33] G. Liu, S. Ye, P. Yan, F. Xiong, P. Fu, Z. Wang, Z. Chen, J. Shi, C. Li, Enabling an integrated tantalum nitride photoanode to approach the theoretical photocurrent limit for solar water splitting, Energy Environ. Sci. 9 (2016) 1327–1334.
[34] I. Perez, J.L.E. Carrejo, V. Sosa, F.G. Perera, J.R.F. Mancillas, J.T.E. Galindo, C.I. R. Rodríguez, Evidence for structural transition in crystalline tantalum pentoxide films grown by RF magnetron sputtering, J. Alloys Compd. 712 (2017) 303–310.
[35] M.J. Axley, A. Böck, T.C. Stadtman, Catalytic properties of an Escherichia coli formate dehydrogenase mutant in which sulfur replaces selenium, Proc. Natl. Acad. Sci. 88 (1991) 8450–8454.
[36] K. Hoelsch, I. Sührer, M. Heusel, D. Weuster-Botz, Engineering of formate dehydrogenase: synergistic effect of mutations affecting cofactor specificity and chemical stability, Appl. Microbiol. Biotechnol. 97 (2013) 2473–2481.
[37] A. Alissandratos, H.-K. Kim, H. Matthews, J.E. Hennessy, A. Philbrook, C.J. Easton, Clostridium carboxidivorans strain P7T recombinant formate dehydrogenase catalyzes reduction of CO_2 to formate, Appl. Environ. Microbiol. 79 (2013) 741–744.
[38] S.K. Kuk, R.K. Singh, D.H. Nam, R. Singh, J.K. Lee, C.B. Park, Photoelectrochemical reduction of carbon dioxide to methanol through a highly efficient enzyme cascade, Angew. Chemie Int. Ed. 56 (2017) 3827–3832.
[39] P.J. Elving, W.T. Bresnahan, J. Moiroux, Z. Samec, NAD/NADH as a model redox system: mechanism, mediation, modification by the environment, Bioelectrochem. Bioenerg. 9 (1982) 365–378.
[40] Gul Rahman, Jiyeon Lim, Kwang-Deog Jung, O.-S. Joo, Electrodeposited Ru nanoparticles for electrochemical reduction of NAD^+ to NADH, Int. J. Electrochem. Sci. 6 (2011) 2789–2797.
[41] Y. Chen, P. Li, H. Noh, C.-W. Kung, C.T. Buru, X. Wang, X. Zhang, O.K. Farha, Stabilization of formate dehydrogenase in a metal–Organic framework for bioelectrocatalytic reduction of CO_2, Angew. Chemie Int. Ed. 58 (2019) 7682–7686.
[42] T. Saba, J.W.H. Burnett, J. Li, P.N. Kechagiopoulos, X. Wang, A facile analytical method for reliable selectivity examination in cofactor NADH regeneration, Chem. Commun. 56 (2020) 1231–1234.
[43] M.C. McCormick, K. Keijzer, A. Polavarapu, F.A. Schultz, M.-H. Baik, Understanding intrinsically irreversible, non-nernstian, two-electron redox processes: a combined experimental and computational study of the electrochemical activation of platinum(IV) antitumor prodrugs, J. Am. Chem. Soc. 136 (2014) 8992–9000.
[44] Y.H. Kim, Y.J. Yoo, Regeneration of the nicotinamide cofactor using a mediator-free electrochemical method with a tin oxide electrode, Enzyme Microb. Technol. 44 (2009) 129–134.

[45] I. Schröder, E. Steckhan, A. Liese, In situ NAD^+ regeneration using 2,2′-azinobis(3-ethylbenzothiazoline-6-sulfonate) as an electron transfer mediator, J. Electroanal. Chem. 541 (2003) 109–115.
[46] F. Man, S. Omanovic, A kinetic study of NAD^+ reduction on a ruthenium modified glassy carbon electrode, J. Electroanal. Chem. 568 (2004) 301–313.
[47] L. Wang, X. Zhou, N.T. Nguyen, I. Hwang, P. Schmuki, Strongly enhanced water splitting performance of Ta_3N_5 nanotube photoanodes with subnitrides, Adv. Mater. 28 (2016) 2432–2438.
[48] J. Tian, R. Ning, Q. Liu, A.M. Asiri, A.O. Al-Youbi, X. Sun, Three-dimensional porous supramolecular architecture from ultrathin g-C_3N_4 nanosheets and reduced graphene oxide: solution self-assembly construction and application as a highly efficient metal-free electrocatalyst for oxygen reduction reaction, ACS Appl. Mater. Interfaces 6 (2014) 1011–1017.
[49] D.A. Lutterman, Y. Surendranath, D.G. Nocera, A self-healing oxygen-evolving catalyst, J. Am. Chem. Soc. 131 (2009) 3838–3839.
[50] L. Reijnders, M. Huijbregts, Biofuels for Road Transport: A Seed to Wheel Perspective, Springer Science & Business Media, 2008.
[51] H. Hirakawa, M. Hashimoto, Y. Shiraishi, T. Hirai, Photocatalytic conversion of nitrogen to ammonia with water on surface oxygen vacancies of titanium dioxide, J. Am. Chem. Soc. 139 (2017) 10929–10936.
[52] A.F. Ciftja, A. Hartono, H.F. Svendsen, Experimental study on carbamate formation in the AMP–CO_2–H_2O system at different temperatures, Chem. Eng. Sci. 107 (2014) 317–327.
[53] S. Ferri, K. Kojima, K. Sode, Review of Glucose Oxidases and Glucose Dehydrogenases: A Bird's Eye View of Glucose Sensing Enzymes, SAGE Publications, 2011.
[54] C. Wandrey, Biochemical reaction engineering for redox reactions, Chem. Rec. 4 (2004) 254–265.
[55] I. Ali, A. Gill, S. Omanovic, Direct electrochemical regeneration of the enzymatic cofactor 1,4-NADH employing nano-patterned glassy carbon/Pt and glassy carbon/Ni electrodes, Chem. Eng. J. 188 (2012) 173–180.
[56] G. Morello, B. Siritanaratkul, C.F. Megarity, F.A. Armstrong, Efficient electrocatalytic CO_2 fixation by nanoconfined enzymes via a C3-to-C4 reaction that is favored over H2 production, ACS Catal. 9 (2019) 11255–11262.
[57] M. Miller, W.E. Robinson, A.R. Oliveira, N. Heidary, N. Kornienko, J. Warnan, I.A. C. Pereira, E. Reisner, Interfacing formate dehydrogenase with metal oxides for the reversible electrocatalysis and solar-driven reduction of carbon dioxide, Angew. Chemie Int. Ed. 58 (2019) 4601–4605.
[58] Q. Wang, J. Warnan, S. Rodríguez-Jiménez, J.J. Leung, S. Kalathil, V. Andrei, K. Domen, E. Reisner, Molecularly engineered photocatalyst sheet for scalable solar formate production from carbon dioxide and water, Nat. Energy 5 (2020) 703–710.
[59] S.Y. Lee, S.Y. Lim, D. Seo, J.-Y. Lee, T.D. Chung, Light-driven highly selective conversion of CO2 to formate by electrosynthesized enzyme/cofactor thin film electrode, Adv. Energy Mater. 6 (2016), 1502207.
[60] V. Andrei, B. Reuillard, E. Reisner, Bias-free solar syngas production by integrating a molecular cobalt catalyst with perovskite–$BiVO_4$ tandems, Nat. Mater. 19 (2020) 189–194.